Adaption of artificial microvascular networks

Thierry Fredrich Michael Welter Heiko Rieger

January 25, 2019

Abstract

We explored the application of the adaption algorithm introduced by Secomb et. al. to artificial blood vessel networks and find that the resulting networks to not obey Murray's law. The reported analysis and visual examples document the contrast between two different types of networks. We conjecture that an interrupt of an established signaling cascade could be a hallmark of solid vascular tumors.

Contents

1 Introduction **3**

2 Methods **3**
2.1 The adaption algorithm . . . 3
2.2 The artificial blood vessel networks. . . . 4
2.3 Particle Swarm optimization . . . 4

3 Results **5**
3.1 Convergence . . . 5
3.2 Signal distribution . . . 5
3.3 Murray's law . . . 5
3.4 Quantitative analysis . . . 14

4 Discussion **14**

5 Conclusion **16**

A Reproducing available data **17**

1 Introduction

Physicists have always been fascinated by nature with its perfect shapes optimized by years of evolution to fulfill diverse range of tasks.

Nowadays, a lot of models follow the idea of activator and inhibitor as introduced by the famous paper of Turing in 1952 ([Tur52]). The sophisticated review [KM94] documents a lot of ideas where the quantitative predictions of Turings model are used to explain multiple patterns observed in nature.

But even before, Cecil Murray proposed a model [Mur26] to describe her observations as biologist on blood vessel networks. She found that the cube of a parent vessel's radius equals the sum of the cubes of the daughter vessel's radii. Later, this law was generalized (see equation 1, compare figure 1) and used not only for blood vessel networks, but for all kind of transport networks [She81]. Certainly the application of Murray's law culminates in the production of bio material based on the formula [ZSW+17].

$$r_c^\alpha = r_a^\alpha + r_b^\alpha \tag{1}$$

Nevertheless its superior application to networks with a strong hierarchy, the formula differs when hierarchy is present but less pronounced e.g. for the microvascular or the vascular bed. Beginning with their first paper in 1995 [PSG95], Pries and Secomb et. al. published a series of papers where they proposed a new way to regulate the radii of the vasculature including the microvascular bed. We describe this model in the main part (section 2.1).

The authors of [MAC06], [MMA+09] included the adaption algorithm into their study to incorporate the change of vessel radii during solid tumor growth. In this work we focus the application of the adaption algorithm to artificial arterio venous networks created by Tumorcode ([FWR18]).

2 Methods

2.1 The adaption algorithm

In [PSG98], the authors present a way to dynamically regulate vessel radii within arterio- venous networks. They construct a feedback loop between the spatial position of the vessels (topology) and their biological functions including hydrodynamics, shear stress and metabolism of of surrounding tissue.

For an elaborated review and some applications of the method see [SDP12]. We briefly summarize the five signals forming the key elements of the algorithm.

S1 - Shear stress A vessel is supposed to shrink whenever the wall shear stress falls below 1 dyne/cm^2 = 10^{-4} kPa and expanding otherwise. When using dyne as unit, the logarithm offers the right dependence.

$$S_1 = \log_{10}(\tau_\mathrm{w}) \tag{2}$$

S2 - Blood pressure The second signal is created by the force acting on a vessel wall. To this end the authors of [PSG98] used a heuristic dependence derived in their previous publications. Due to the lack of better knowledge, we apply this formula as well.

$$S_2 = -\log_{10}\left(100 - 86\exp\left[-5000\left\{\log_{10}\left(\log_{10}(P)\right)\right\}^{5.4}\right]\right) \tag{3}$$

S3 - Metabolic demand The mathematical structure of S3 leads to expansion for small vessels with higher metabolic demand ($Q_\mathrm{ref} > HQ$) i.e. the capillaries and decrease for regions which exceed the reference flow ($Q_\mathrm{ref} < HQ$) i.e. big veins .

$$S_3 = k_\mathrm{m}\log_{10}\left(\frac{Q_\mathrm{ref}}{HQ}\right) \tag{4}$$

k_m is a model constant (compare table 1) and a priori not known. The introduced reference flow is biologically motivated by a minimal flow of RBCs which should always be maintained.

S4 - Topological position S_4 gives rise to the position of the vessels within the entire network structure. The signal propagates from the place where the vessels interact most with the surrounding tissue: the capillary bed. While the downstream propagation from a capillary to a draining root transports consumed chemicals away from there place of interaction, the upstream signaling is less obvious, but recent studies confirmed that vessels send electrical signals within their endothelial layer.

We look at a single Y-shaped intersection and label the three vessels with a,b,c. In the arterial branch a mother vessel has two downstream vessels whereas in the venous branch a daughter vessel has two upstream mothers respectively. The signal is calculate in a recursive fashion by

$$S_c = S_{3,a} + S_{3,b} + S_{4,a}\exp(-x_a/L) + S_{4,b}\exp(-x_b/L) \tag{5}$$

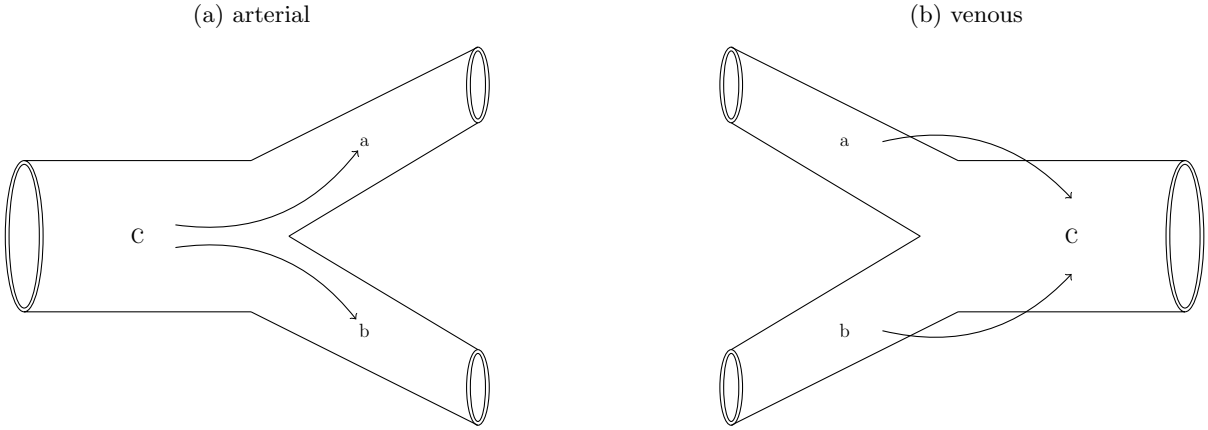

Figure 1: Illustration of the conductive signal propagation. Left: arterial case. Right venous case. Arrows indicate the direction of information propagation. See text and equation 5.

The length of the segments (x_a and x_b) is normalized by an arbitrary model parameter L in the exponential. To account for possible nonlinearities, a saturation to S_0 is used. The complete conductive signal becomes:

$$S_4 = k_\mathrm{c} \frac{S_c}{S_c + S_0} \tag{6}$$

Note that k_c, S_0 and L are unknown model parameters (compare table 1).

S5 - Shrinking tendency Secomb et al. propose that vessels will shrink in the absence of any other stimulation due to the laziness of the endothelial layer. This is embedded in the formula by subtracting a overall constant k_s.

$$S_5 = -k_\mathrm{s} \tag{7}$$

In the model of Secomb et al. the change of a vessel radius is proportional to the sum of the presented signals (S1 - S5). The equation becomes

$$\boxed{\Delta r = S_{tot}\ r\ \Delta t} \text{ with } S_{tot} = \sum_{i=1}^{5} S_i \tag{8}$$

It is obvious that the summation in equation 8 and the construction of the topological signal (S4) form a set of complex and highly nonlinear equations.

2.2 The artificial blood vessel networks.

Since the adaptation algorithm was designed to deal with experimentally measured topologies, there is no further instructions on how to choose the spatial arrangement of the segments in question. Our software [FWR18] allows to construct artificial 3D arterio- venous networks. We report the complete methodology in [RFW16] and summarize the main steps here.

First, at least one arterial and one venous root node have to be distributed in space and assigned with either a blood pressure value or a flow rate. By using a hierarchical iteration scheme, the distribution of capillaries within the given space is optimized. Since the resulting radii are are governed by murrays law, we will call them **M-networks**from now on.

For the scope of this paper, we consider "Rootnode Configuration 4" (RC 4) where one artery is opposite one vein on the x-axis (Compare RC4 in figure 4 of [WFRR16]). To conduct our studies we keep the topology of the **M-network** and adapt the vessel radii according to the model described in section 2.1. For reference we will call successfully adapted networks **A-networks**from now on.

2.3 Particle Swarm optimization

Inspecting section 2.1, we count six unknown parameters for the model (summarized in table 1) and considering the additional hydrodynamic boundary conditions at the root nodes, we end up with may degrees of freedom. This and the fact that we apply the described model in a new context vitiates the possibility to apply the parameters obtained by fitting to rat mesentery. Anyway the published parameters provide a guess about the dimension and we decide to adapt the values of $Q_\mathrm{ref} = 40$, $L = 1500$ and $S_0 = 20$ without change. To identify the other parameters we conduct a particle swarm optimization in the range of 0.5 to 4.0. As reasonable biological objective we choose to minimize the variance in capillary flow.

signal	parameters	parameters fixed by [PSG98]
S_3	k_m	Q_{ref}
S_4	k_c	L, S_0
S_5	k_s	

Table 1: Free parameters of the model. The values in the right column are copied from the cited publication.

label	k_m	k_c	k_s
I	0.83	2.74	1.79
II	0.63	3.19	1.57
III	0.97	2.85	1.79

Table 2: Parameters used to apply the adaption algorithm to the artificial blood vessel networks.

The hydrodynamic boundary conditions at the inlet and outlet of the network needs to be fixed before the optimization. We varied the outlet pressure between 0.5-9.0 kPa and the inlet flow from $10^7 - 10^8$ $\mu m^3/s$ to cover a biological relevant range. To fully utilize the parallel nature of the particle swarm optimization and to distribute the load over 20 Nodes with 320 CPUs of a standard computing cluster, we used the python packages deap ([FRG+12]) and Scoop ([HGGP14]). Details can be obtained from the complete source code at https://github.com/thierry3000/tumorcode After we successfully determined the convergent range of boundary conditions, we chose to keep a pressure of 2.8 kPa at the venous outlet, a flow of 2e7 $\mu m^3/s$ at the arterial inlet and applied the adaption algorithm to 10 independent realizations of RC 4 networks of lateral size 1500 μm constructed with a single hierarchical iteration.

Inspired by the parameter set I, II and II in [PSG98], we applied the adaption procedure to the 10 independent samples with the parmeters reported in table 2.

3 Results

After we successfully reproduced the results on a measured data set (see appendix A), we identified boundary conditions where the adaption algorithm is converged by means of particle swarm optimization, created an ensemble of 10 **M-networks**s which were subsequently used as base to construct an ensemble of 10 **A-networks**that could be analyzed.

3.1 Convergence

As discussed in [PSG98], there are 2 possible outcomes if one applies the adaption scheme in a repeated manner: either one reaches an equilibrium steady state where the changes of radii become arbitrary small with increasing iteration or the changes increase to unrealistic values which also implies unrealistic values for pressure and flow.

By systematic variation (particle swarm optimization 2.3) we identified the networks hydrodynamic boundary conditions were the adaptation algorithm converges and identified the parameter regime to study. The convergent boundary conditions are visualized in figure 2. In total we obtained 253 convergent sets were each set gives rise to the best choice for parameters (k_m, k_c and S_5). The associated distribution is summarized in a box plot (figure 3).

3.2 Signal distribution

Akin to figure A1 and A2, we take the sample with id no. 5 from the ensemble of **A-networks**s and plot: a) the conductive and metabolic signals in figure 4; b) the hydrodynamic signal in figure 5; and c) the hydrodynamic characteristics in figure 6. Due to the construction of the signaling cascade and the convergence of the algorithm, we are not surprised that the distributions of the signals look qualitatively similar.

However the distribution of radii changes from the **M-networks**(bottom left figure 7) to **A-networks**(bottom right column of figure 7), the distribution of the blood pressure does no change because of the fixed boundary conditions (color of top row in figure 7). Since the adaption changes the radii, the flow needs to be modified accordingly! We model the shear force proportional to the flow. Therefore the distribution of the shear force looks similar to the distribution of flow as show in the center row of figure 7. In the bottom row of figure 7 we colored the vessel by their radii which highlights the result of the adaption algorithm.

In figure 7 we compare **M-networks**s (left column) to **A-networks**s (right column). In figure 8 we show data that is only available in the adaption case. In agreement with model assumptions, the metabolic signal is highest at the thin capillaries and the conductive signal is highest at the most distal points.

3.3 Murray's law

By construction the **M-networks**fulfill Murray's law (equation 1). We found that **A-networks**do not fulfill Murray's law (see figure 9 and the inset).

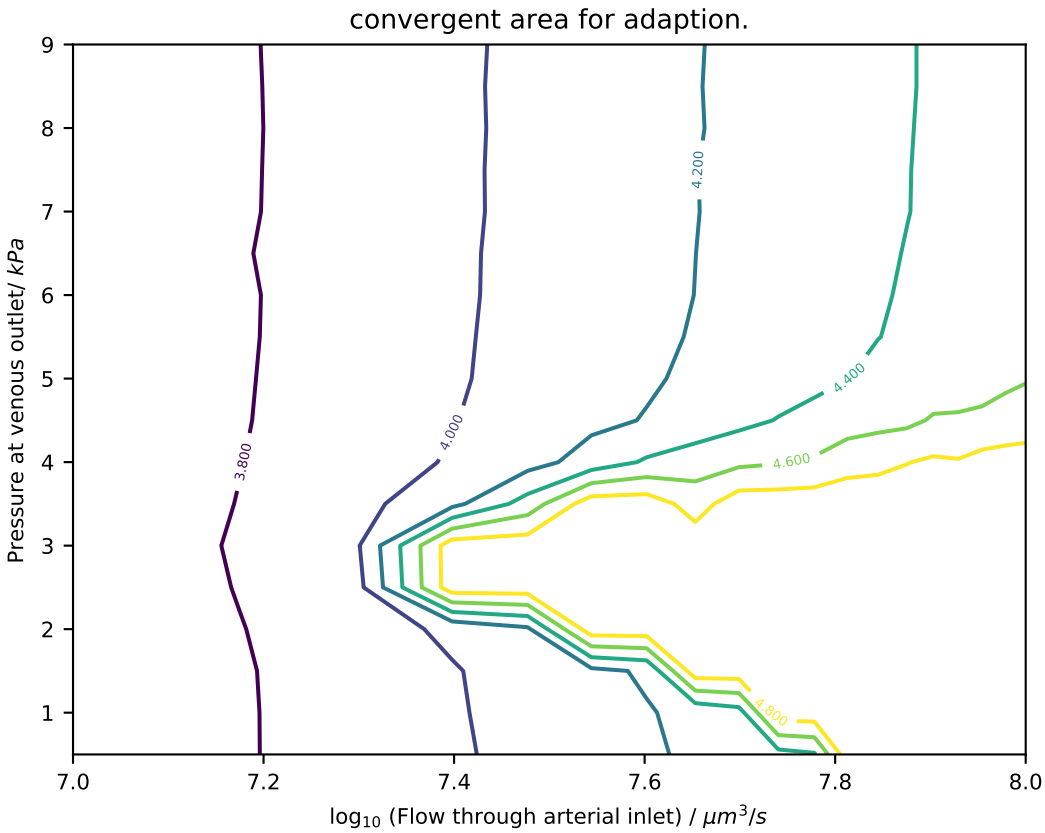

Figure 2: Contour plot showing the log_{10} of the fitness value from the particle swarm optimization i.e. the log_{10} of the standard deviation of the average capillary flow. The x- axis represents the boundary condition at the arterial inlet in logarithmic scale. The y- axis represents the boundary condition at the venous outlet.

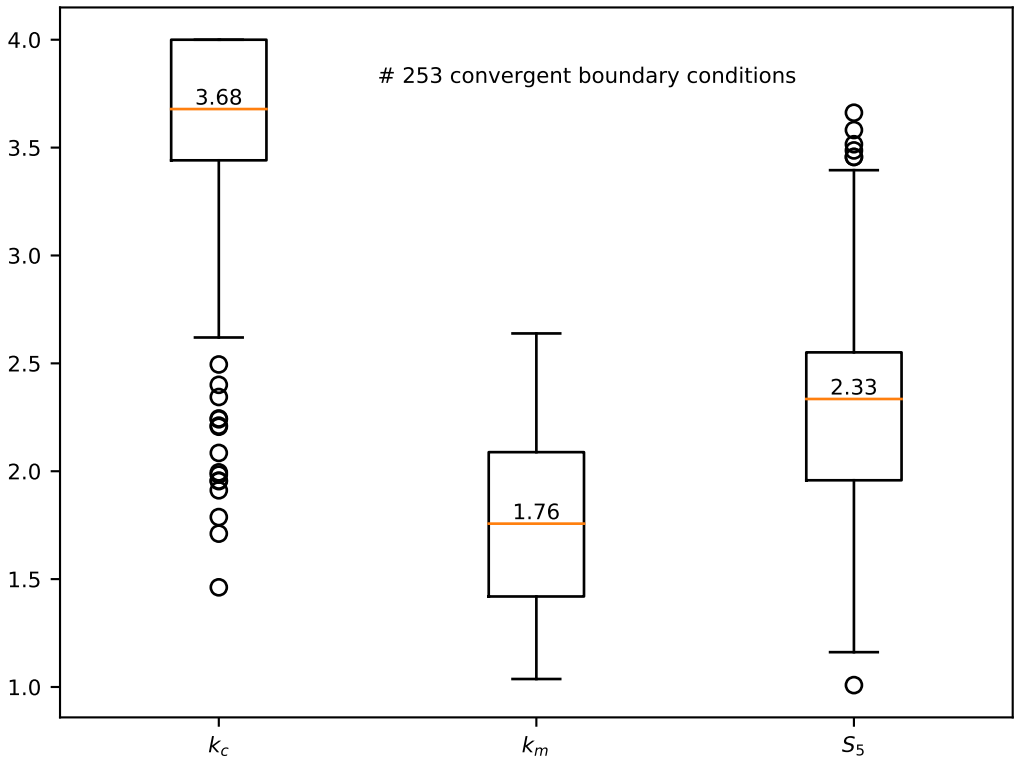

Figure 3: Boxplot summarizing the best choice for k_m , k_c and k_s as obtained by particle swarm optimization. Only convergent data sets are considered. The median value is write above the corresponding line.

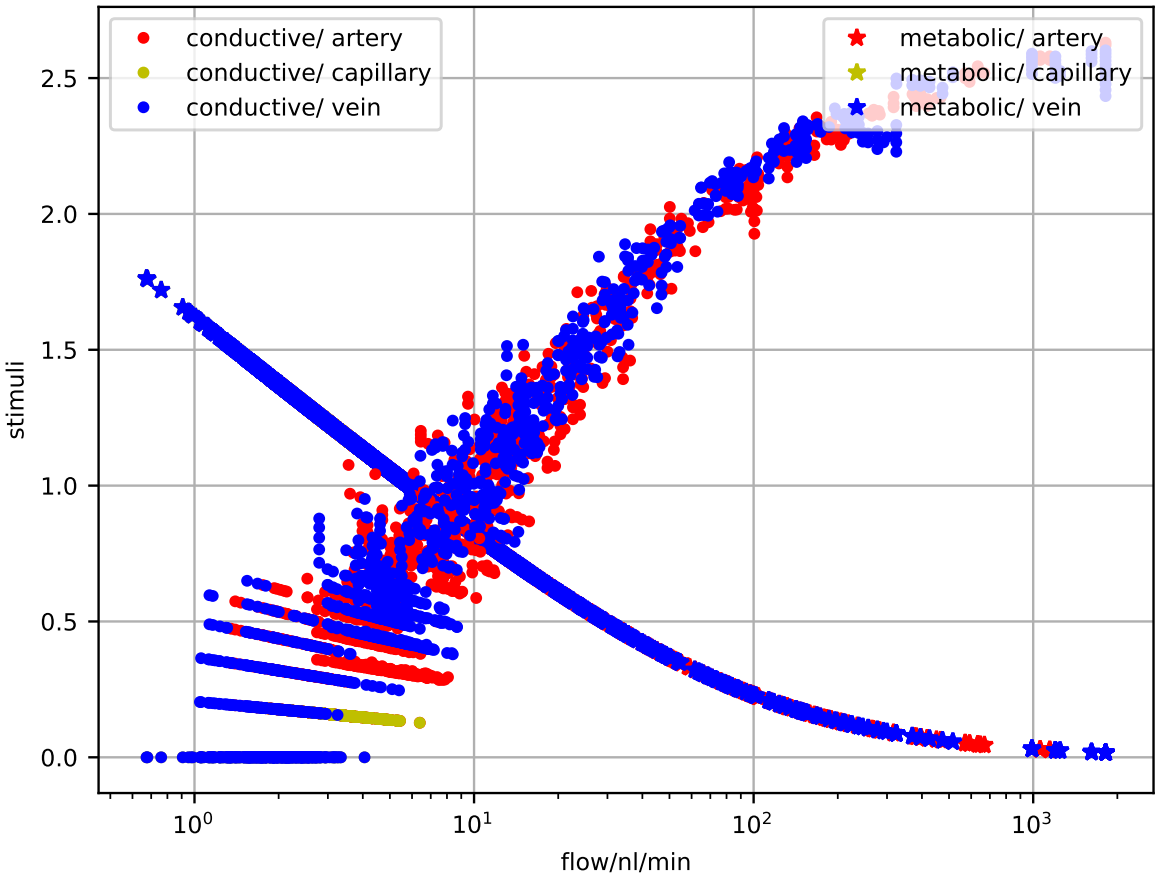

Figure 4: Akin to figure 5 lower row in [PSG98], this figure shows the strength of the adaption stimuli based on the conductive and the metabolic signal. Metabolic signals are indicated by asterisks and conductive signals by bullets. The color is based on the vessel type store by Tumorcode.

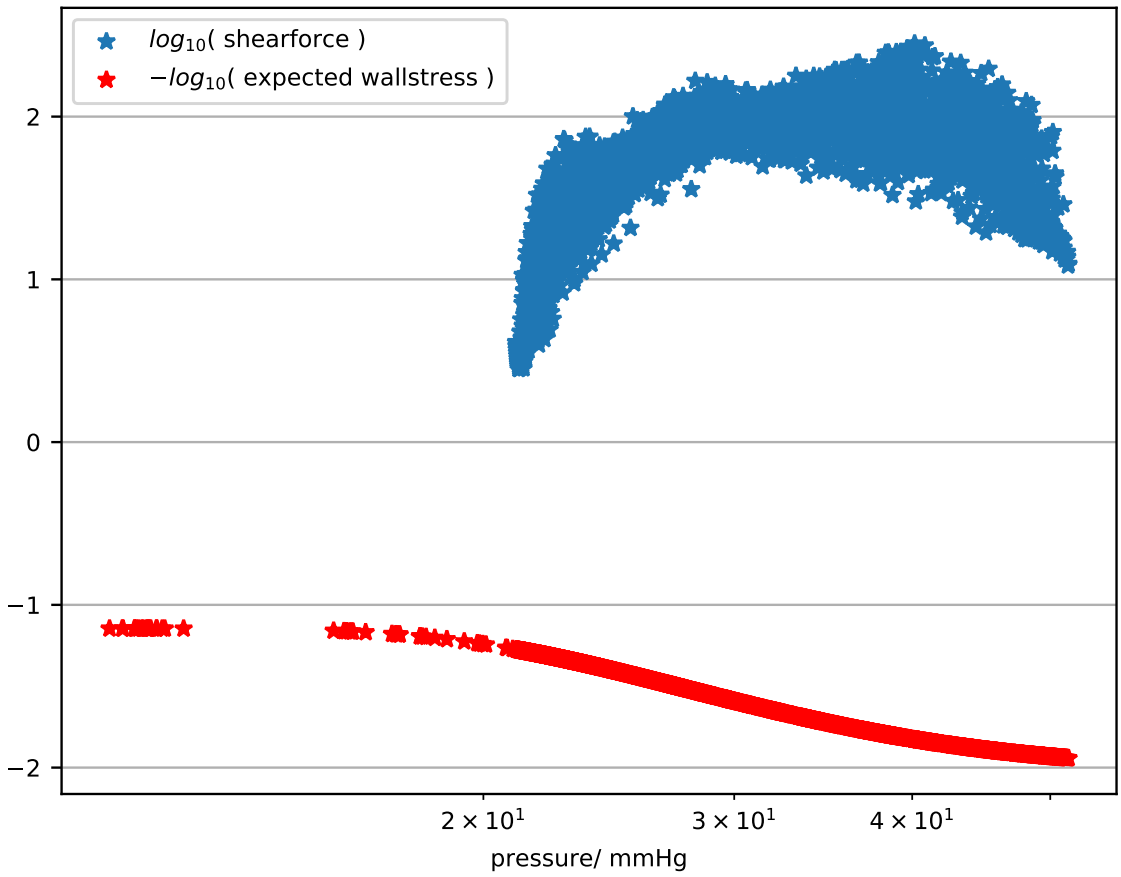

Figure 5: Akin to figure 5 B) in [PSG98], this figure shows the hydrodynamic stimuli derived from the shear force (τ_w) and the pressure P

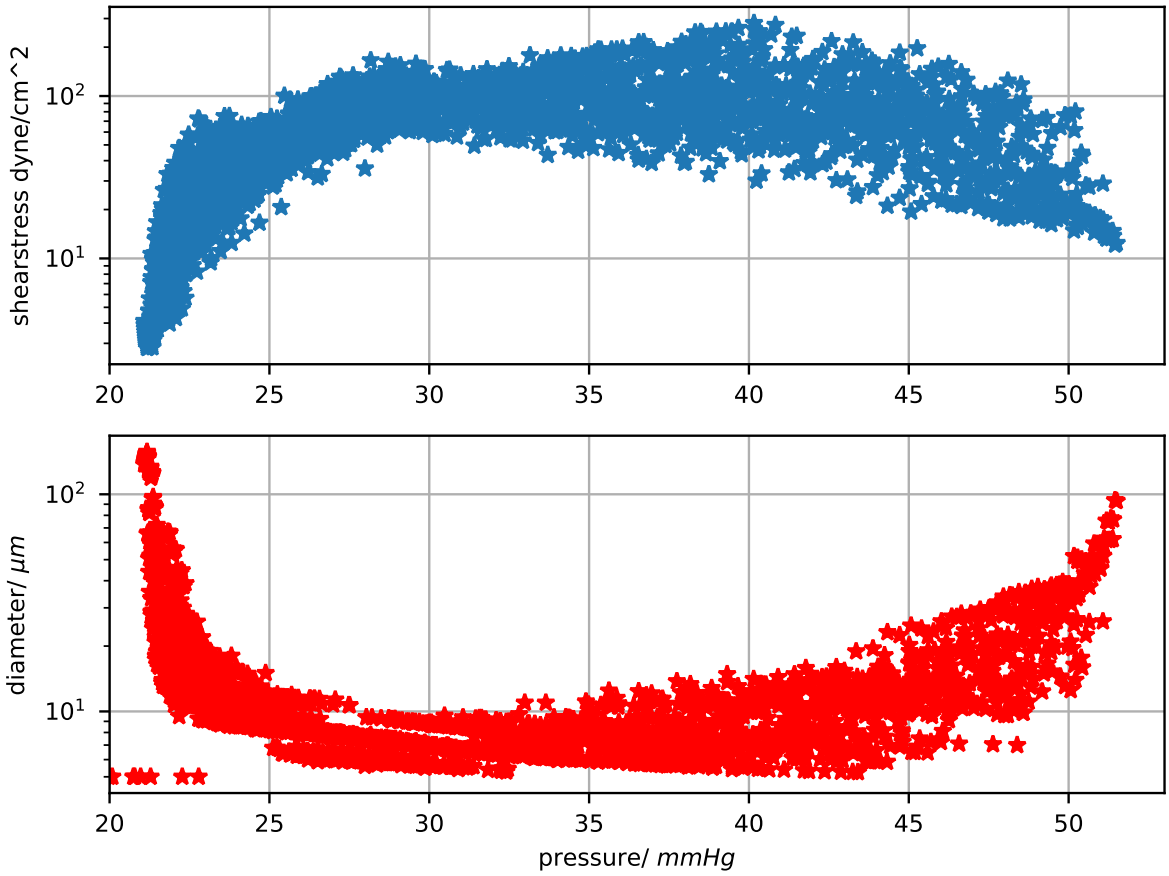

Figure 6: Akin to figure 4 lower row in [PSG98], this figure shows characteristic hemodynamic and morphological parameters of the **M-networks**with id 5. In the top row the acting shear stress is plotted along the vessels blood pressure. In the bottom row the vessel diameter is plotted along the vessels blood pressure.

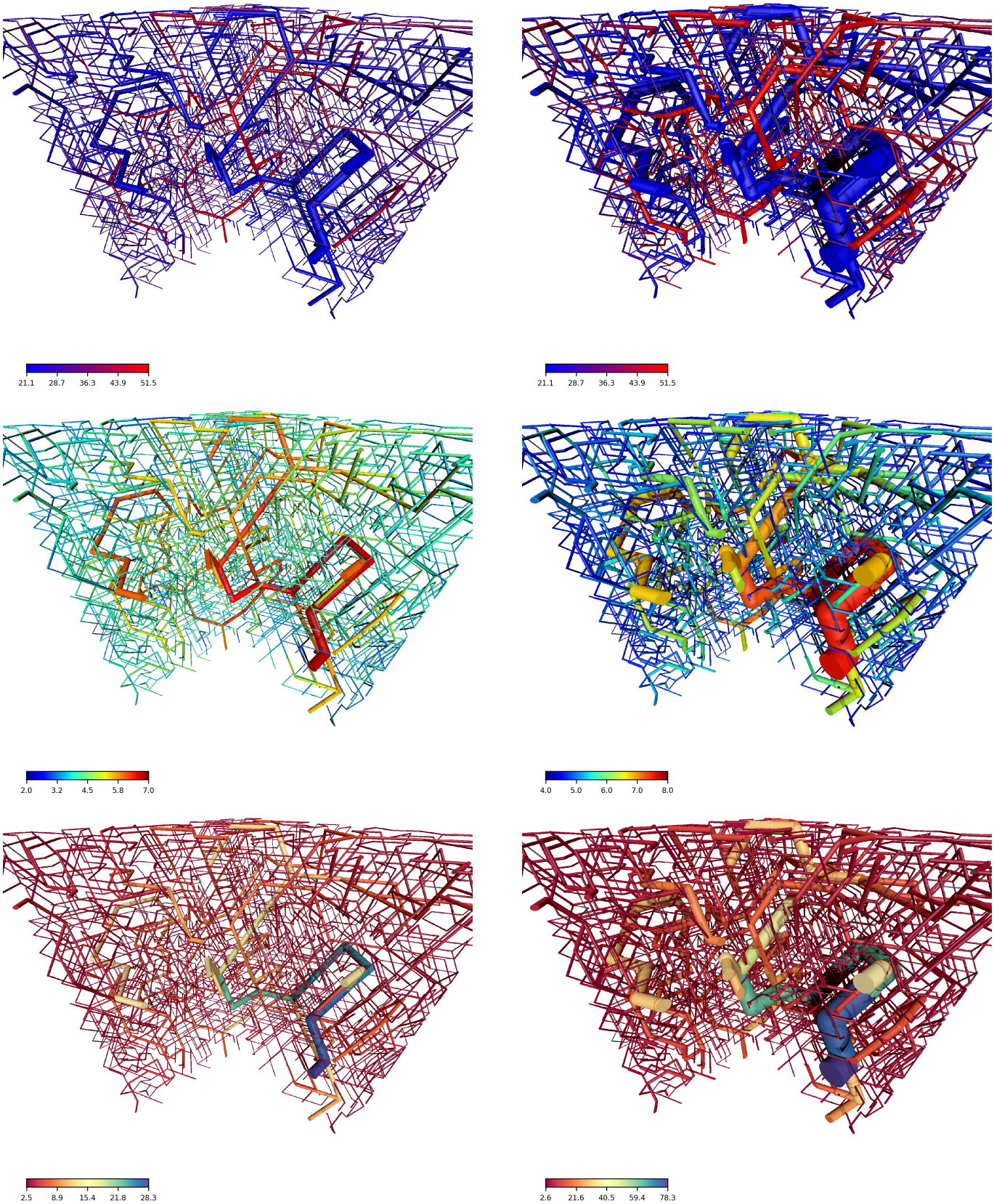

Figure 7: Color coded vessel properties for network with id 5. From top to bottom: pressure in mmHg, shear force in *log*, radius in μm. Left column show the **M-networks**and the right column depict the **A-networks**.

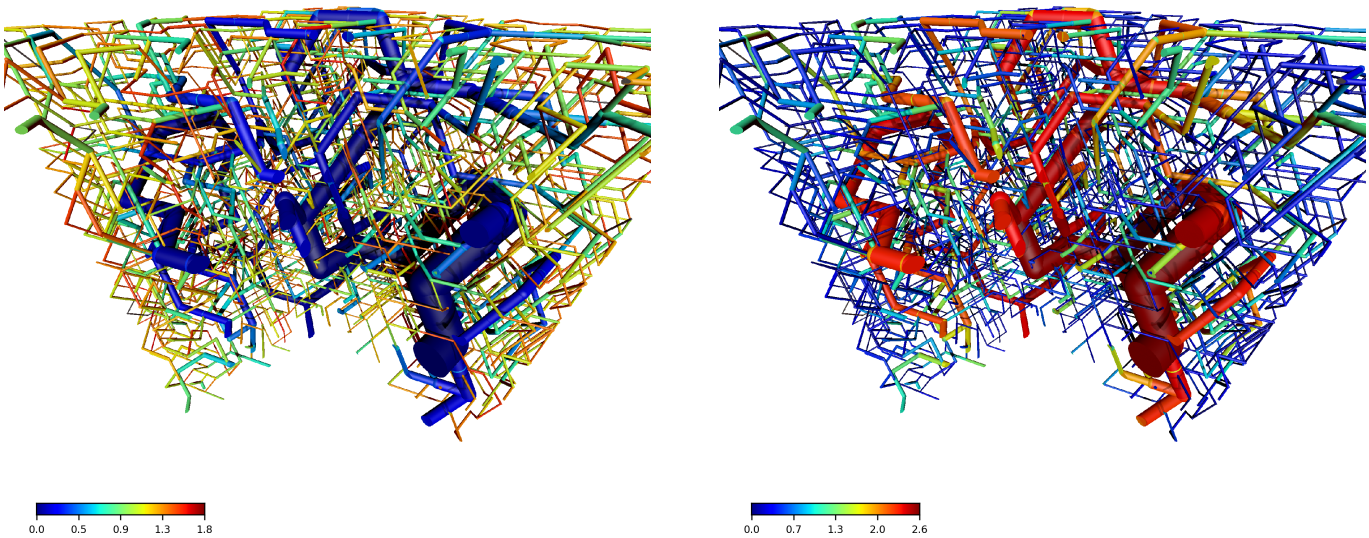

Figure 8: The figure shows vessel properties that are only available in the adaption case for the network from the ensemble with id 5. Left column: metabolic signal as calculated in equation 4. Right column: conductive signal as calculated in equation 5.

Despite its simple appearance, the dependence in murray's law is tricky. In figure 10 we look at every possible intersection within the network and check the differences between left and right branch for a representative of **M-networks**(in the left panel) and a representative of **A-networks**(in the right panel). We find that this distribution is smooths out by the adaption and becomes much broader (see abscissa of figure 10).

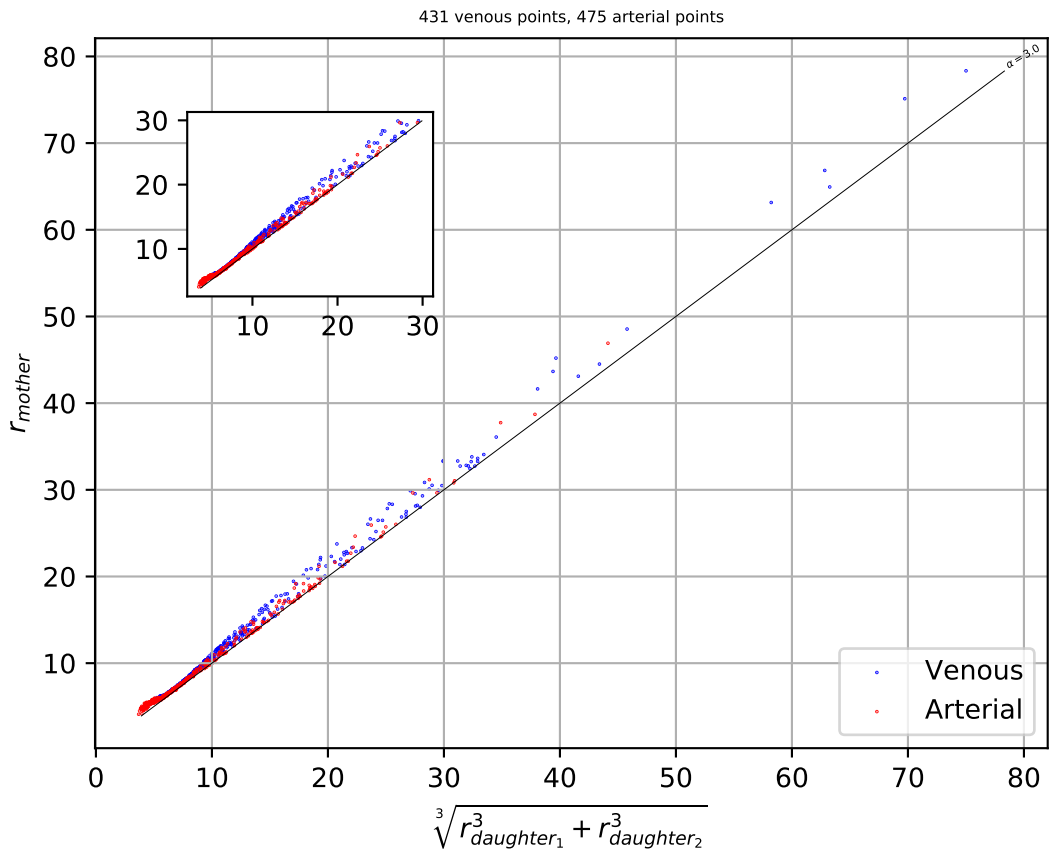

Figure 9: The black diagonal represents murray's law for $\alpha = 3$. The data points are taken from the convergent data set with id 5. Blue dots are venous intersections and red dots are arterial intersections. The inset shows the same curve at lower values (see axis).

(a) Tumorcode

(b) adaptation

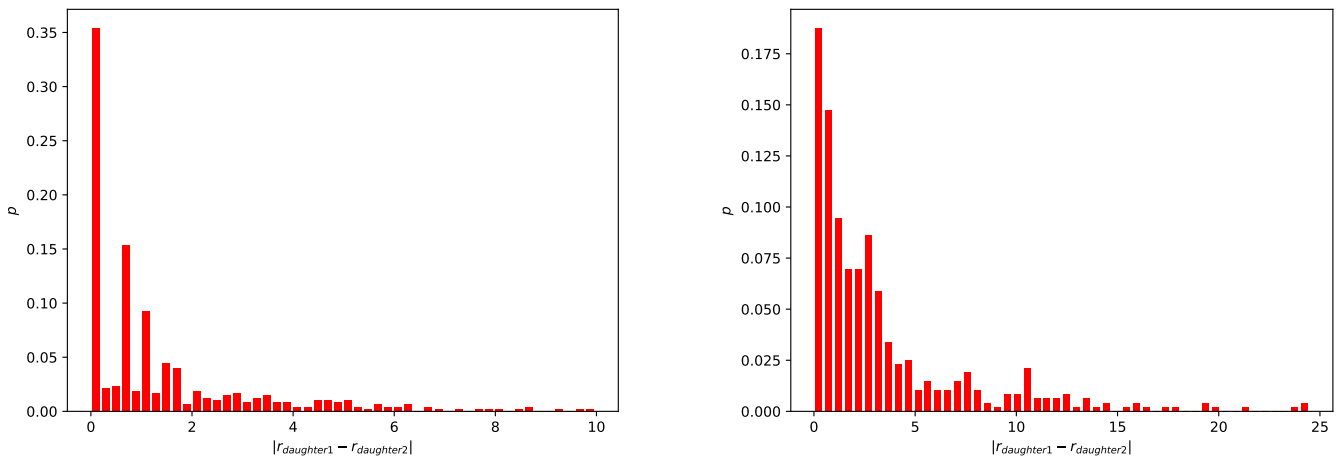

Figure 10: Normalized distribution of differences between two daughter vessels at a Y- shaped intersection. In both cases the representative with id 5 is used. Left column: **M-networks**. Right column: **A-networks**obtained with parameterset I.

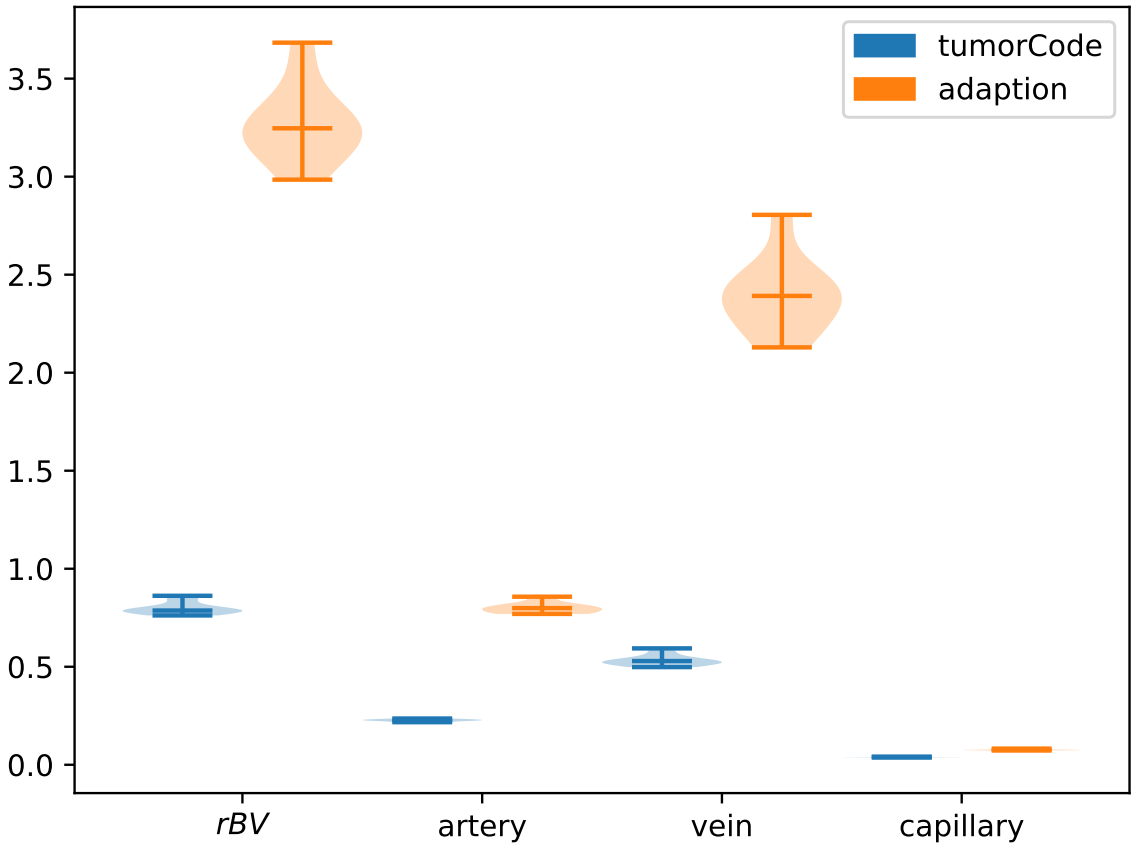

Figure 11: The reginal blood volume (rBV) is averaged over 10 network samples and shown by percent. From left to right the data for all vessels, only arteries, only veins and only capillaries is shown. The blue color is used for the M-networks before adaption and orange is used for the adapted networks. Note that artery, vein and capillary add up to the rBV entry.

3.4 Quantitative analysis

We determined the regional blood volume (rBV) and the surface to volume ratio for each of the 10 samples before (**M-networks**) and after the adaption (**A-networks**). For the **A-networks**, the rBV is more than 3 time higher than for the **M-networks**(see figure 11). While the contributions from arteries and veins vary significantly, the contribution from the capillaries are about the same.

Considering the surface to volume ratio (figure 12), Tumorcode creates networks with a higher ratio resulting in a better biological efficiency. Note that the s2v ratio is highest for the capillaries in the M-networks.

We conclude that the optimization arranging the capillaries in Tumorcode fulfills its purpose: namely to create a homogeneous environment for nutrient exchange.

4 Discussion

The algorithm in question (section 2.1) was designed to assess data sets obtained from animal models. Unfortunately such data is still very rare. We applied the the adaption scheme to artificial blood vessel networks obtained by Tumorcode. In contrast to previous approached, we could not fit to measured data sets to obtain the free parameters (compare table 1) . Therefor we exploit PSO to estimate the parameters under reasonable assumptions which are a) biological boundary conditions (inflow and pressure at outlet) and b) homogeneous distribution of hydrodynamics within the capillary bed.

The radii in the convergent data sets do <u>not</u> follow Murray's law (9 and 10). Murray's law includes two aspects of energy that balance each other to the famous formula, but the concept of adaption includes more than two aspects of energy. In the adaption algorithm the hydrodynamic energies are augmented by a form of electrical or topological energy (conductive signal) and chemical energies (metabolic signal) which have to be minimized mutually. From figure 7 and 8 in section 3.2 and the data in section 3.4 it becomes apparent how the the two presented types of vessel

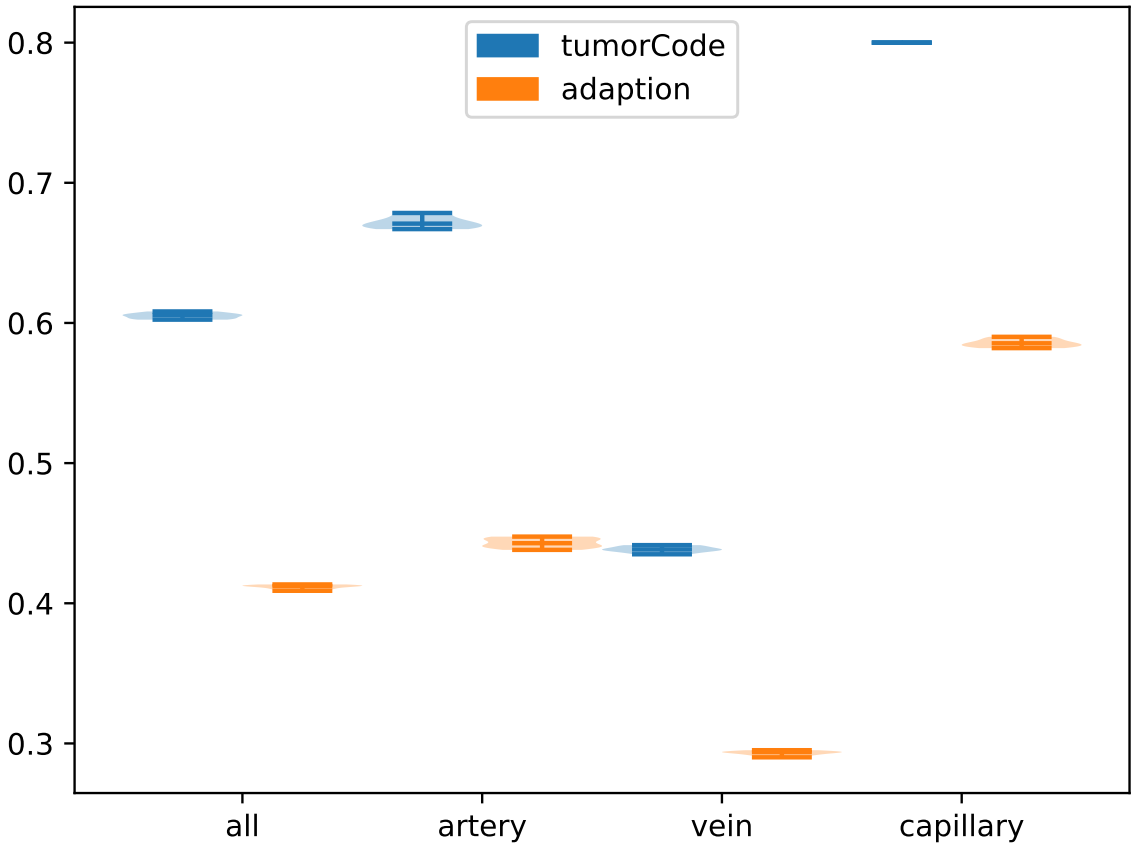

Figure 12: The surface to volume ratio (s2v) is averaged over 10 network samples. From left to right the data for all vessels, only arteries, only veins and only capillaries is shown. The blue color is used for the M-networks before adaption and orange is used for the adapted networks.

networks differ. A quantitative analysis of regional blood volume (rBV) and surface to volume ratio (s2v) showed that the **A-networks**carry more blood while the **M-networks**offer a higher surface to volume ratio — especially at the capillary level.
We failed adding the algorithm to the implementation of vascular tumor growth in Tumorcode (data not shown). For a fixed set of adaption parameters, the convergence was not stable while vessel regression or angiogenesis happened. In those cases the conductive signal was interrupted or shared between new vessels and prevented convergence. Others who used the adaption algorithm in the realm of tumor growth resigned to use the conductive signal at all. We could not find an explanation why they neglected this in their work. In contrast, it is stated in [MAC06]:

> "These stimuli form a basic set of requirements in order to obtain stable network structures with realistic distributions of vessels diameters and flow velocities."

while Pries and Secomb [PSG98] stated that:

> "..., it is necessary to introduce a further stimulus that reflects the topological position of a segment in the networks, ..."

and

> "These tests confirmed that all four stimuli were needed to prevent strong strong deviations of ..."

Authors remark: they talk about four signals because the do not count the constant shrinking (k_s) as separate signal. Those facts let us worry about their results.

5 Conclusion

We applied the adaption algorithm introduced by Secomb et. al. in [PSG98] to synthetic arterio- venous networks. To our knowledge such an application was not done before because the selection of the free parameters was restricted to experimental data. In future, when computers become even more powerful, the application of non linear optimization techniques such as the presented particle swarm optimization will allow to retrace the construction of arterio- venous networks — and more questions occuring in nature.

The signals introduce by the adaption algorithm provide an intersection to the ever increasing understanding of basic biological processes and mathematical modelling. Currently the signals are modeled with parameters (the free parameters in our description, compare table 1), but what if those signals become experimentally accessible input in future? The model is ready and once the drop in voltage along a vessel or its metabolic uptake are measurable, we can fix the parameters.

In future work, we hope to understand the feedback between vascular tumors, the adption signals and the topology of blood vessels in tissue.

k_c	2.74
k_m	0.83
k_s	1.99*
Q_{ref}	40
S_0	20
Δt	0.1*

Table 3: Parameter used to adapt radii of rat mesentery network with Tumorcode. Parameters labeled by * are not the same as in the publication of [PSG98], see text.

(a) initial

(b) after convergence

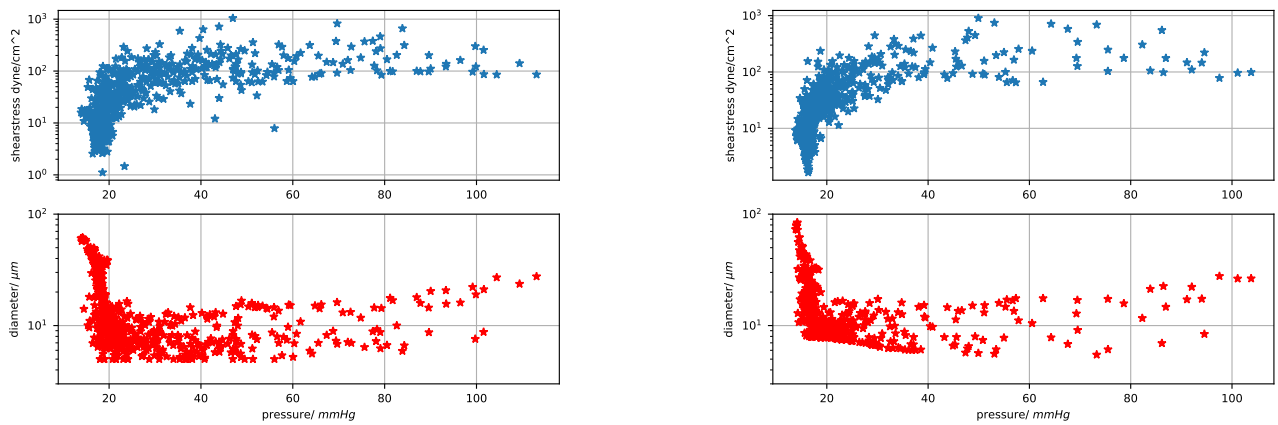

Figure A1: Distribution of characteristic hemodynamic and morphological parameters. Column a) before and column b) after convergent adaptation. The top row shows the shear stress as a function of the blood pressure. Lower row shows the vessel diameter likewise as function of the blood pressure. Note that the ordinate is on logarithmic scale.

A Reproducing available data

We applied our implementation of the adaption algorithm to the network published by Pries et al. [PSG98]. They measured the hydrodynamic boundary conditions which we incorporate accordingly. Unfortunately a differential time step is stated but not documented — we used $\Delta t = 0.1$. Furthermore it was not sufficient to use exactly the same parameters as documented Secomb et al. We achieve convergence we changed k_s from 1.79 to 1.99 in our simulations. We believe this required since our calculation of the hemodynamics is more advanced and therefore results in slightly different behavior.

To check our implementation we reproduced figure 4 and 5 of [PSG98]. Due to the lack of quantitative data, we cannot compare directly, but we find that figure A1 is in qualitative agreement with its original.

Figure A2 (top row, left) lacks negative values for the logarithm of the shear force. Obviously our model does not include such a case. The lower row of figure A2 is in qualitative agreement with [PSG98]. Here we accomplished the plot with information about the type of vessels (artery, capillary or vein) which is required in Tumorcode, but not stated in the original data.

(a) initial

(b) after convergence

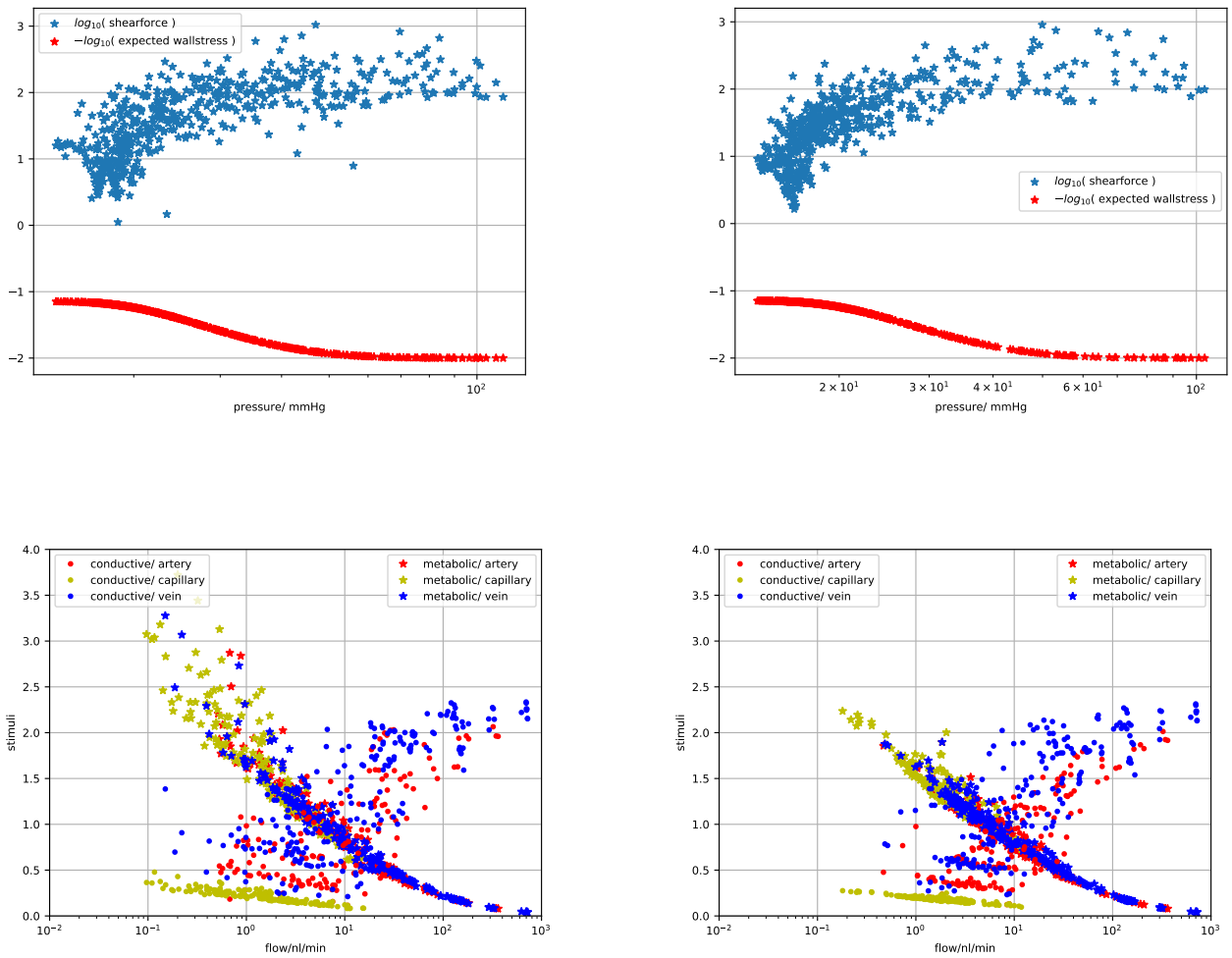

Figure A2: Signals contributing to the total adaptation signal of the rat mesentery network consisting of 546 segments. Left column shows the signal strength at the beginning of the adaptation procedure and the right column the situation once convergence is reached. Upper row depicts the hydrodynamic parts of the signal. S_1 derived from the shear force in blue. S_2 derived from the transmural pressure in red. Lower row depicts the metabolic and conductive parts which corresponds to S_3 and S_4. Colors interpret the type of the vessel which could be either artery, vein or capillary.

References

[FRG+12] Félix-Antoine Fortin, François-Michel De Rainville, Marc-André Gardner, Marc Parizeau, and Christian Gagné. DEAP: Evolutionary Algorithms Made Easy. *Journal of Machine Learning Research*, 13:2171–2175, July 2012.

[FWR18] Thierry Fredrich, Michael Welter, and Heiko Rieger. Tumorcode. *Eur. Phys. J. E*, 41(4):55, April 2018.

[HGGP14] Yannick Hold-Geoffroy, Olivier Gagnon, and Marc Parizeau. Once You SCOOP, No Need to Fork. In *Proceedings of the 2014 Annual Conference on Extreme Science and Engineering Discovery Environment*, XSEDE '14, pages 60:1–60:8, New York, NY, USA, 2014. ACM.

[KM94] A.J. Koch and Hans Meinhardt. Biological Pattern-Formation—From basic mechanisms to complex structures. *Reviews of Modern Physics*, 66:1481, October 1994.

[MAC06] Steven R. McDougall, Alexander R. A. Anderson, and Mark A. J. Chaplain. Mathematical modelling of dynamic adaptive tumour-induced angiogenesis: Clinical implications and therapeutic targeting strategies. *Journal of Theoretical Biology*, 241(3):564–589, August 2006.

[MMA+09] Paul Macklin, Steven McDougall, Alexander R. A. Anderson, Mark A. J. Chaplain, Vittorio Cristini, and John Lowengrub. Multiscale modelling and nonlinear simulation of vascular tumour growth. *J. Math. Biol.*, 58(4):765–798, April 2009.

[Mur26] Cecil D. Murray. The Physiological Principle of Minimum Work. *Proc Natl Acad Sci U S A*, 12(5):299–304, May 1926.

[PSG95] A. R. Pries, T. W. Secomb, and P. Gaehtgens. Design principles of vascular beds. *Circ. Res.*, 77(5):1017–1023, November 1995.

[PSG98] A. R. Pries, T. W. Secomb, and P. Gaehtgens. Structural adaptation and stability of microvascular networks: theory and simulations. *American Journal of Physiology - Heart and Circulatory Physiology*, 275(2):H349–H360, August 1998.

[RFW16] Heiko Rieger, Thierry Fredrich, and Michael Welter. Physics of the tumor vasculature: Theory and experiment. *Eur. Phys. J. Plus*, 131(2):31, February 2016.

[SDP12] Timothy W. Secomb, Mark W. Dewhirst, and Axel R. Pries. Structural Adaptation of Normal and Tumour Vascular Networks. *Basic Clin Pharmacol Toxicol*, 110(1):63–69, January 2012.

[She81] T. F. Sherman. On connecting large vessels to small. The meaning of Murray's law. *The Journal of General Physiology*, 78(4):431–453, October 1981.

[Tur52] Alan Mathison Turing. The chemical basis of morphogenesis. *Phil. Trans. R. Soc. Lond. B*, 237(641):37–72, August 1952.

[WFRR16] Michael Welter, Thierry Fredrich, Herbert Rinneberg, and Heiko Rieger. Computational Model for Tumor Oxygenation Applied to Clinical Data on Breast Tumor Hemoglobin Concentrations Suggests Vascular Dilatation and Compression. *PLOS ONE*, 11(8):e0161267, August 2016.

[ZSW+17] Xianfeng Zheng, Guofang Shen, Chao Wang, Yu Li, Darren Dunphy, Tawfique Hasan, C. Jeffrey Brinker, and Bao-Lian Su. Bio-inspired Murray materials for mass transfer and activity. *Nature Communications*, 8:14921, April 2017.